Available online at www.sciencedirect.com
ScienceDirect
Trans. Nonferrous Met. Soc. China 34(2024) 966−976
Transactions of Nonferrous Metals Society of China
www.tnmsc.cn

Refining mechanisms of arsenic during preparation process of ultrafine WC powder by nitridation−carbonization method

Zhi-qiang YI[1], Dun-qiang TAN[1,2]

1. School of Physics and Materials Science, Nanchang University, Nanchang 330031, China;
2. International Institute of Materials Innovation, Nanchang University, Nanchang 330031, China

Received 14 September 2022; accepted 18 May 2023

Abstract: To simplify the preparation process and prepare ultrafine WC powder, a certain amount of As element was added to the ammonium paratungstate precursor. The mechanism of As in the preparation process of ultrafine WC powder by nitridation−carbonization method was systematically discussed. The results show that when the carbonization temperature was 1400 °C, the nitridation temperature increased from 500 to 600 °C, and the As content increased from 0 to 0.3 wt.%, the average particle size of the prepared WC powder decreased from 2.23 to 0.22 μm, and the particle uniformity was significantly improved. The As element in the nitrided product was in the form of $W_2O_3(AsO_4)_2$, which was easily enriched or distributed between the two phases on the surface of the nitrided products $(NH_4)_{0.42}WO_3$ and WN, hindering the growth of WC grains during the carbonization process. Consequently, ultrafine WC powder was prepared.
Key words: arsenic; ultrafine WC powder; uniformity; refining mechanism; nitridation; carbonization

1 Introduction

Ultrafine-grained WC−Co cemented carbide has excellent properties such as high strength, high hardness, special wear resistance and fracture toughness. It is widely used in cutting tools, mining machinery and corrosion-resistant parts [1−5]. The grain size and uniformity of WC in ultrafine WC−Co cemented carbide are not only related to the sintering process, but also depend on the particle size and uniformity of WC powder. Therefore, preparing ultrafine WC powder with good dispersion and uniform particles is the key technology to obtain high-performance ultrafine WC−Co cemented carbide [6−10].

In the traditional production process of WC powder, ammonium paratungstate (APT) or ammonium metatungstate (AMT) is mainly used as raw material. WC powder was obtained by calcination, hydrogen reduction and carbonization. The phase transition stage is APT→$(NH_4)_xWO_3$→WO_3→$WO_{2.9}$→$WO_{2.72}$→WO_2→W→W_2C→WC [11−13]. In the process of hydrogen reduction of tungsten oxide (WO_x), due to the presence of H_2, volatile $WO_2(OH)_2$ will be generated when tungsten and its oxides contact with water vapor. The homogeneous reduction reaction of $WO_2(OH)_2$ with H_2 occurs after volatilization, and the generated reduction products are deposited on the nucleated tungsten grains, thereby promoting the growth of tungsten powder particles [14−16]. Studies have shown that the direct reduction−carbonization method can be used to prepare WC powder with a primary particle size of submicron or even nanometer [17−20]. STANCIU et al [21] milled tungsten oxide and carbon black for 48 h to obtain WC powder with particle size of 20−30 nm, and the time can be shortened to 30 h by high-energy ball milling. However, this method is inefficient and not suitable

Corresponding author: Dun-qiang TAN, Tel: +86-791-83968963, E-mail: tdunqiang@ncu.edu.cn
DOI: 10.1016/S1003-6326(23)66446-5

for large-scale industrial production. MA and ZHU [22] fully milled WO_3 and graphite, and then calcined at 1215 °C to obtain ultrafine WC powder with a particle size of 169 nm. Unfortunately, the lower carbonization temperature will lead to the abnormal growth of WC grains in the subsequent preparation of WC−Co cemented carbide. In addition, the reduction−carbonization of tungsten oxide using gas carbon sources such as CH_4, CO, $CO + CO_2$ or $CH_4 + H_2$ is also an effective method for preparing ultrafine tungsten carbide [23−26]. However, since the gaseous reduction carbonization agent and tungsten oxide in the static reaction system cannot be fully contacted, the obtained product is prone to carbon-deficient phase W_2C, so it is unsuitable for industrial production. These are the problems existing in the actual production of ultrafine tungsten carbide.

On the other hand, among the many impurity elements in scheelite, arsenic (As) content is high, usually in the form of AsO_4^{3-} and $HAsO_4^{2-}$ [27,28]. In industrial production, As is generally used as a harmful impurity element and is removed [29]. However, the previous research results of our research group showed that nano-W powder with uniform particle size, ultrafine WC powder and ultrafine WC−Co cemented carbide with excellent performance can be prepared by adding a certain amount of As element to APT through the calcination, hydrogen reduction, carbonization and sintering [30,31]. Since As can provide the nucleation core for the nucleation of W powder in the hydrogen reduction process of tungsten oxide, whether As can also refine WC powder in the process of direct preparation of WC powder by nitridation−carbonization method has not been reported at home and abroad.

In this work, single phase or multiphase tungsten compounds ($(NH_4)_xWO_3$, WN, etc.) containing As were prepared by nitridation−carbonization method. The effects of As on the phase composition of $(NH_4)_xWO_3$ and WN and the mechanism of WC powder refinement during nitridation−carbonization were studied. In this method, ultrafine WC powder with uniform particle size can be prepared by only two steps of nitridation and carbonization using APT as raw material. The addition of As in raw materials provides a theoretical basis for eliminating the impurity removal process in the tungsten metallurgy process.

2 Experimental

2.1 Sample preparation

Figure 1 shows the schematic diagram of the preparation process of ultrafine WC powder. Firstly, 0.3 g As was dissolved into 65−68 wt.% nitric acid, and then 99.7 g APT (purity >99.9%, mean particle size ~37.5 μm) was added to the nitric acid solution containing As, fully stirred and then placed in a vacuum oven for drying treatment. The temperature was set to be 80 °C and the time was about 12 h. The dried APT precursor containing As was placed in an agate mortar for grinding and crushing treatment, and then packed with an alumina crucible and placed in a tube furnace. Ammonia gas was introduced into the furnace for nitridation treatment, and the nitridation temperature was 500 or 600 °C to obtain the nitrided product. The nitrided products at different temperatures were carbonized according to the corresponding stoichiometric ratio, and then mixed by a planetary ball mill. The uniformly

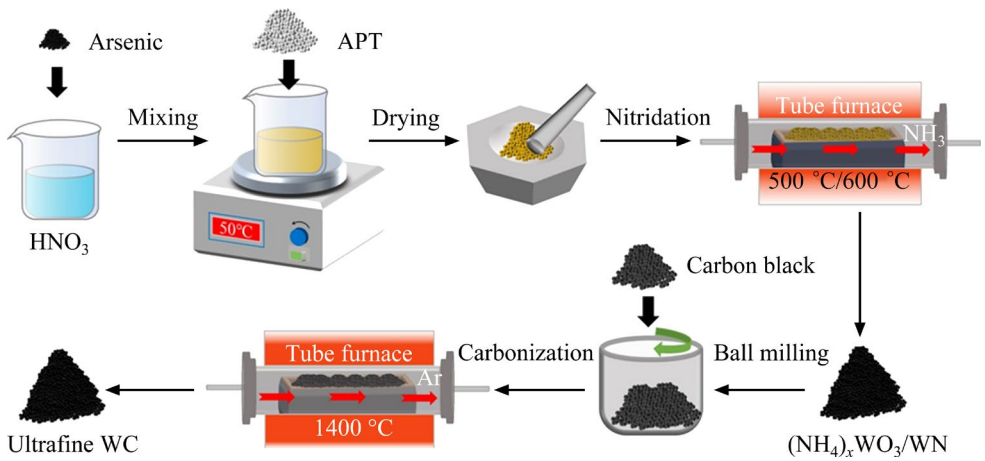

Fig. 1 Schematic diagram of preparation process of ultrafine WC powder

mixed composite powders were carbonized in a high temperature tube furnace, and Ar gas was introduced into the furnace as a protective gas. The ultrafine WC powder was prepared by carbonization at 1400 °C for 2 h.

2.2 Characterization

The chemical phases of nitridation and carbonization products were studied by X-ray diffractometer (XRD, PANalytic, EMPYREAN). The equipment used a copper target (Cu K_α), and the accelerating voltage and current were 40 kV and 40 mA, respectively. The morphology and microstructure of the samples were characterized using an analytical field emission scanning electron microscope (FESEM, Nova Nano SEM 450 FEI), an energy dispersive spectrometer (EDS, INCA energy 250 X-max 50 Oxford Instruments) and a high-resolution transmission electron microscope equipped with energy dispersive (HRTEM, JEM−2100F JEOL). The size distribution of WC particles was measured by Nano Measurer software.

3 Results and discussion

3.1 Nitrided powder

Figures 2(a) and (b) show the XRD patterns of the APT and APT−0.3%As precursors after nitridation at 500 and 600 °C in NH_3 atmosphere, respectively. The nitridation products of APT and APT−0.3%As were both $(NH_4)_{0.25}WO_3$ (JCPDS No. 73-1084), and there were almost no diffraction peaks of other phases when the nitridation temperature was 500 °C. This indicated that the phase formed by nitridation of APT and APT−0.3%As at 500 °C in NH_3 atmosphere was $(NH_4)_{0.25}WO_3$ single phase, and the diffraction peak of the second phase containing As was not detected in the nitridation product of APT−0.3%As. This was because the addition of As in APT−0.3%As was only 0.3 wt.%. Furthermore, some As was volatilized in the form of gaseous As_2O_3 during heating [31], so the content of As remaining in $(NH_4)_{0.25}WO_3$ cannot be detected. The diffraction peak of the product was obviously broadened when the nitridation temperature was 600 °C. Through phase analysis, it was found that the nitridation products of APT and APT−0.3%As mainly contained WN (JCPDS No. 65-2898) and $(NH_4)_{0.42}WO_3$ (JCPDS No. 42-0451). Through comparing the diffraction peak intensity, it can be found that the main phase in the nitridation product of the control sample was WN, while the content of $(NH_4)_{0.42}WO_3$ was less. The strongest peak diffraction intensities of WN and $(NH_4)_{0.42}WO_3$ in APT−0.3%As nitridation products were similar.

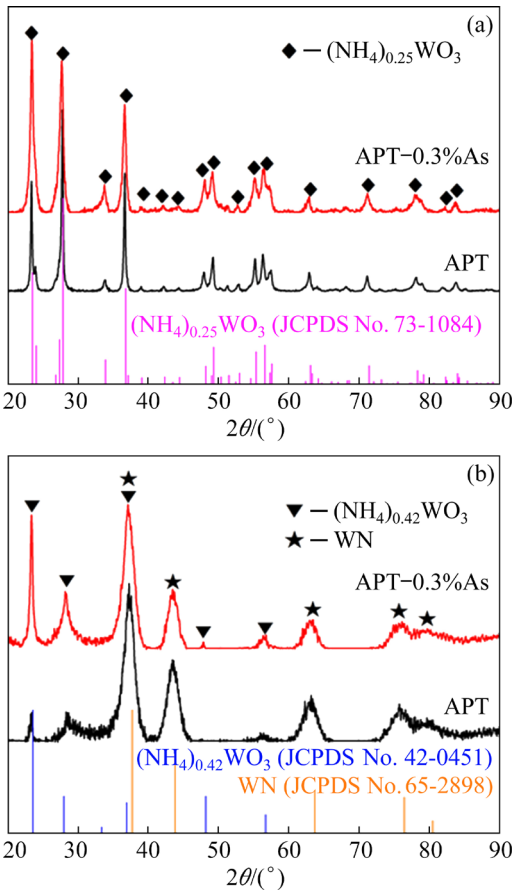

Fig. 2 XRD patterns of APT and APT−0.3%As at different nitridation temperatures: (a) 500 °C; (b) 600 °C

Figure 3 shows the SEM morphologies and EDS analysis results of the products prepared by APT or APT−0.3%As after nitridation at 500 and 600 °C. The nitrided product of APT at 500 °C is $(NH_4)_{0.25}WO_3$. The microstructure of the powder is shown in Fig. 3(a). It can be seen that the morphology and particle size of $(NH_4)_{0.25}WO_3$ are similar to those of APT raw material. The particles are mostly cubes or polyhedrons with smooth surface. However, due to the decomposition of APT during the calcination process, a large amount of ammonia and water vapor were produced, resulting in cracks on the surface. The particle size of $(NH_4)_{0.25}WO_3$−As powder shown in Fig. 3(b) is significantly reduced, and the particle surface is more porous. Figure 3(c) shows the morphology of

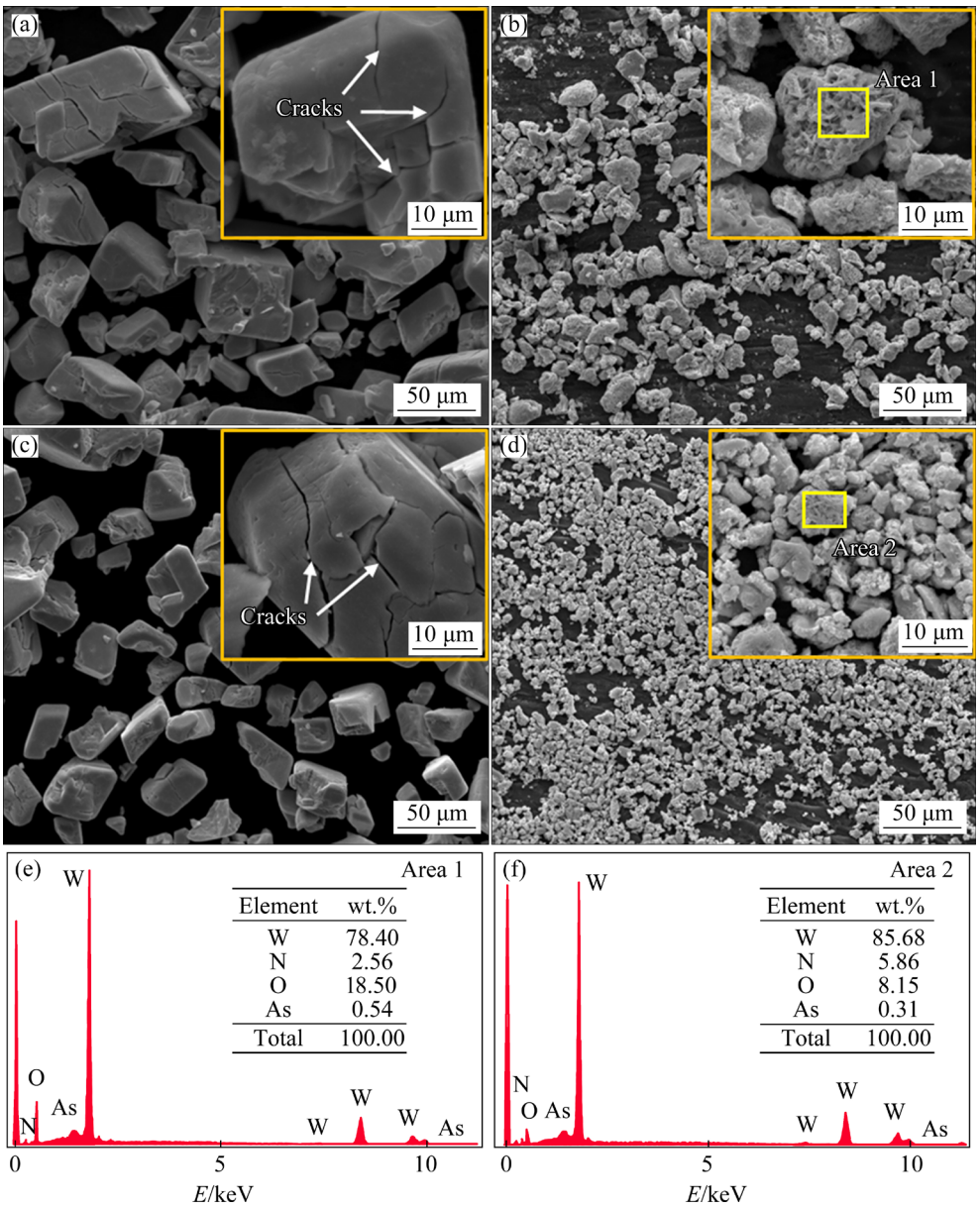

Fig. 3 SEM images and EDS results of calcined products of APT and APT−0.3%As at different temperatures: (a) APT at 500 °C; (b) APT−0.3%As at 500 °C; (c) APT at 600 °C; (d) APT−0.3%As at 600 °C; (e) EDS result of Area 1 in (b); (f) EDS result of Area 2 in (d)

the products (WN and $(NH_4)_{0.42}WO_3$) of APT nitrided at 600 °C. Compared with the nitrided product $(NH_4)_{0.25}WO_3$ at 500 °C in Fig. 3(a), the particle size of the nitrided product at 600 °C decreases. This is because the decomposition of APT is a process of continuous water loss, ammonia loss and volume shrinkage. Therefore, with the increase of calcination temperature, the particle size of the product decreases. By observing the cracks on the surface of the particle, it was found that the number and width of cracks on the surface of the particle increase in Fig. 3(c). This is due to the release of more water vapor and ammonia during the decomposition of APT with increasing temperature, resulting in serious cracking on the surface of the particle. Similarly, the particle size of the nitrided product of APT−0.3%As at 600 °C in Fig. 3(d) is also significantly reduced, and there are many pores on the surface of the powder particles, which is conducive to the rapid escape of water vapor and ammonia during the thermal decomposition process, and can also accelerate the diffusion of carbon atoms in the subsequent carbonization process.

Figures 3(e) and (f) show the element analysis results of Areas 1 and 2 in Figs. 3(b) and (d),

respectively. It was found that the oxygen content in the product was 18.50 wt.% when the nitridation temperature was 500 °C, and the oxygen content in the product was reduced to 8.15 wt.% when the calcination temperature increased to 600 °C because part of $(NH_4)_{0.25}WO_3$ was converted to WN with the increase of temperature. Due to the decrease of oxygen content in the product, the mass fractions of N and W elements in the corresponding Area 1 increased compared to those in Area 2. In addition, the presence of As was detected in Areas 1 and 2, but the content of As in Area 2 was lower than that in Area 1. The reason is that with the increase of nitridation temperature, the content of As volatilized from gaseous As_2O_3 increases, resulting in the decrease of As content.

3.2 Carbonized powder

According to the analysis of the above experimental results, Table 1 describes the phases corresponding to the products prepared by nitridation at 500 and 600 °C in NH_3 atmosphere with APT or APT−0.3%As as raw materials. The WC powders prepared by direct carbonization of four kinds of nitrided products are shown in Table 1. In order to facilitate the distinction of WC prepared by direct carbonization of different nitrided products, they are named as the form in Table 1.

Table 1 Comparison of phases of calcined products at different temperatures and nomenclature of carbonized products

Precursor	Calcination temperature/°C	Product after calcination	Product after carbonization
APT	500	$(NH_4)_{0.25}WO_3$	WC-500
APT−0.3%As	500	$(NH_4)_{0.25}WO_3$−As	WC−As-500
APT	600	WN + $(NH_4)_{0.42}WO_3$	WC-600
APT−0.3%As	600	WN−As + $(NH_4)_{0.42}WO_3$−As	WC−As-600

Figures 4(a−d) show the XRD patterns of WC obtained by direct carbonization of the nitrided products of APT and APT−0.3%As at 500 and 600 °C, respectively. After comparative analysis, it was found that only the diffraction peak of WC (JCPDS No. 51-0939) was detected in the four nitrided products directly carbonized at two different temperatures, and no W_2C phase was detected, indicating that $(NH_4)_{0.25}WO_3$ and $(NH_4)_{0.42}WO_3$/WN can be completely carbonized at 1400 °C for 2 h. The diffraction peaks corresponding to each crystal face of WC are sharp, indicating that the WC particles have good crystallinity. No As-containing phase was detected in the diffraction patterns of WC−As-500 (Fig. 4(b)) and WC−As-600 (Fig. 4(d)). The reason is that the amount of As added in the precursor APT was only 0.3 wt.%. As volatilized in the form of gaseous arsenic oxide during subsequent nitridation and carbonization, and the final residual As content in WC-As-500 and WC-As-600 was low, which was difficult to achieve the accuracy of the X-ray diffractometer.

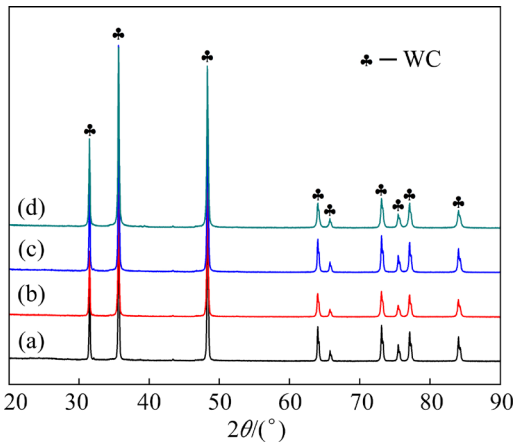

Fig. 4 XRD patterns of WC powders obtained by carbonization of different calcined products: (a) WC-500; (b) WC−As-500; (c) WC-600; (d) WC−As-600

Through Fig. 4, it was found that the addition of As element has no effect on the phase composition of the product after carbonization. In order to reveal the influence of As on the growth of WC grains, the grain size of each WC sample was calculated by using the Debye−Scherrer formula, as shown in Eq. (1):

$$D=\frac{K\lambda}{B\cos\theta} \tag{1}$$

where D is the average grain size in the direction perpendicular to the crystal plane; K is the Scherrer constant; λ is X-ray wavelength, 0.154 nm; B is the full width at half maximum (FWHM) of the measured sample diffraction peak, which needs to be converted to radian (rad); θ is the Bragg diffraction angle [32].

In Fig. 5, the grain sizes of WC-500, WC−As-500, WC-600 and WC−As-600 are 57.7, 47.0, 53.3 and 41.2 nm, respectively. It was found that the grain size of WC−As-500 was significantly smaller than that of WC-500, similarly, the grain size of WC−As-600 was also smaller than that of WC-600. This shows that As has a significant inhibitory effect on the growth of WC grains during the direct carbonization of $(NH_4)_{0.25}WO_3$ or $(NH_4)_{0.42}WO_3$/WN to prepare WC powder.

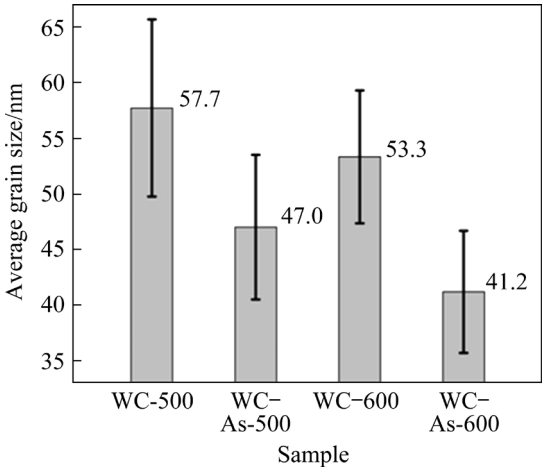

Fig. 5 Average grain size histogram of different WC powders calculated by XRD patterns

Figure 6 shows the SEM images of WC powders prepared by direct carbonization of different nitridation products. Figures 6(a) and (b) show the morphologies of WC-500 and WC−As-500 obtained by carbonization of $(NH_4)_{0.25}WO_3$ and $(NH_4)_{0.25}WO_3$−As with APT and APT−0.3%As at 500 °C, respectively. It is found that the WC-500 (Fig. 6(a)) powder particles are coarse and agglomerated obviously. The agglomeration of WC−As-500 (Fig. 6(b)) powder particles is slightly weakened. There are many smaller primary particles that are not agglomerated, but there are also many coarse secondary aggregates around the small primary particles. Figures 6(c) and (d) show the morphologies of WC-600 and WC−As-600 obtained by the carbonization of $(NH_4)_{0.42}WO_3$/WN and $(NH_4)_{0.42}WO_3$/WN−As nitrided by APT and APT−0.3%As at 600 °C, respectively. At low magnification, WC-600 powders are agglomerates with a size of tens of microns. At high magnification,

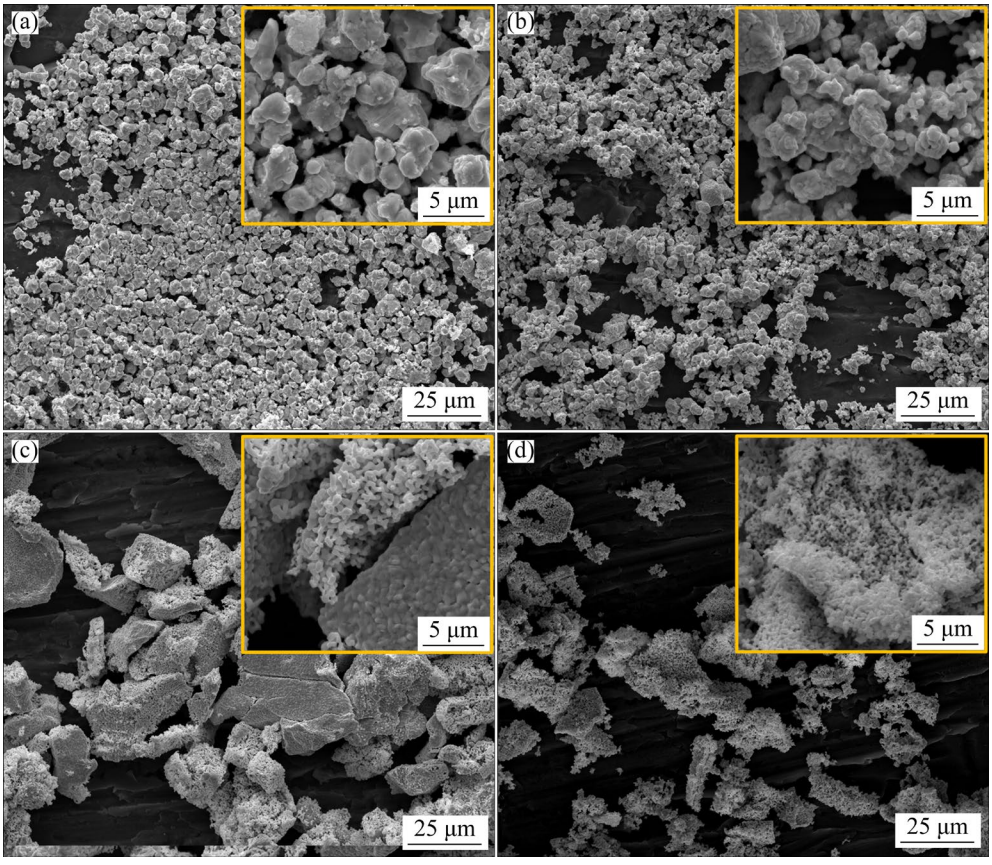

Fig. 6 SEM images of WC powders obtained by carbonization of different calcined products: (a) WC-500; (b) WC−As-500; (c) WC-600; (d) WC−As-600

the coarse WC-600 aggregates are composed of many fine particles with a size of several hundred nanometers. There are many pores between the fine WC primary particles in some coarse aggregates, forming a loose and porous structure. The bonding force between the particles of this structure is weak and it is easy to break during ball milling. In Fig. 6(c), there are also some dense WC aggregates formed by the polymerization of fine WC primary particles. This dense structure has strong binding force and is difficult to break. The WC−As-600 (Fig. 6(d)) powders are almost all loose porous ultrafine WC particles, and the powder uniformity is excellent. This shows that when the nitridation temperature is 600 °C, the nitrided products of $(NH_4)_{0.42}WO_3$ and WN can significantly refine the size of the WC primary particles, and the addition of As element is beneficial to weakening the agglomeration between the WC particles, so as to obtain ultrafine WC powder with uniform particle size and satisfactory dispersion. In addition, the inductively coupled plasma (ICP) detection data show that the As contents in the products WC−As-500 and WC−As-600 are 0.0093 wt.% and 0.0047 wt.%, respectively, which are much lower than the addition amount in the precursor APT, indicating that As will volatilize in a gaseous form during the nitridation and carbonization processes.

Figure 7 shows a histogram of the average particle size of different tungsten carbides. The average particle sizes of WC-500 and WC−As-500 are 2.23 and 1.36 μm, respectively. The average particle size of WC-500 is coarse, and most of the primary WC particles merge and grow through grain boundary migration during high temperature carbonization, resulting in obvious coarsening of WC particles. The average particle size of WC−As-500 decreases, indicating that the addition of As element can hinder the growth or merging of WC−As-500 particles. When the nitridation temperature increased from 500 to 600 °C, the nitrided products of APT and APT−0.3%As changed from single-phase ($(NH_4)_{0.25}WO_3$) to two-phase ($(NH_4)_{0.42}WO_3$ and WN). The average particle sizes of WC-600 and WC−As-600 prepared by direct carbonization of APT and APT−0.3%As at 600 °C are 0.43 and 0.22 μm, respectively. Compared with WC-500 or WC−As-500 powders, the average particle sizes of WC-600 and WC−As-600 decreased significantly. Not only the average particle size of WC−As-600 is smaller than that of WC-600, but also its dispersibility is reduced and the powder uniformity is significantly improved. It is further explained that As element can refine WC particles to prepare ultrafine WC powder with prosperous uniformity.

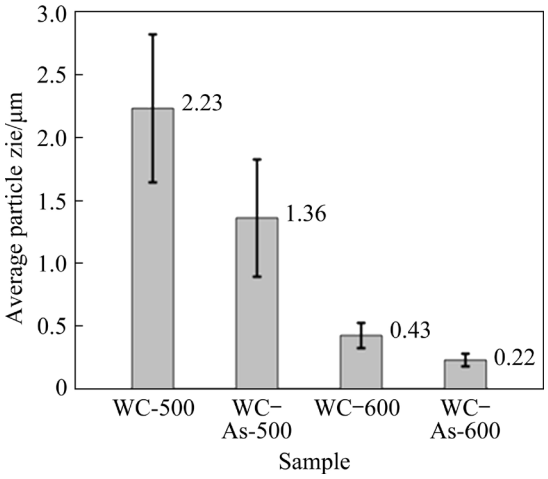

Fig. 7 Average particle size histogram of different WC powders based on SEM images

3.3 Refining mechanism of ultrafine WC powders

Figures 8(a) and (b) show the TEM images of $(NH_4)_{0.42}WO_3$/WN and $(NH_4)_{0.42}WO_3$/WN−As composite powders prepared by nitridation of precursor APT and APT−0.3%As at 600 °C in NH_3 atmosphere, respectively. It can be seen that the $(NH_4)_{0.42}WO_3$/WN powder is coarse, while the $(NH_4)_{0.42}WO_3$/WN−As composite powder is a typical nanocrystalline aggregate with fine and uniform particle size. In order to clarify its phase composition and structure, the powders in the micro-area were selected for electron diffraction. The diffraction patterns showed polycrystalline diffraction rings, indicating that the powder structure in the micro-area was polycrystalline. The polycrystal diffraction rings were calibrated. It was found that the corresponding phases of the two groups of diffraction rings were both WN, and the corresponding WN crystal planes from inside to outside were (111), (200), (220) and (311). The diffraction ring of $(NH_4)_{0.42}WO_3$ was not detected in the selected regions of Figs. 8(a) and (b). Possibly due to the low content of $(NH_4)_{0.42}WO_3$ in the micro-area, the brightness of the diffraction ring was darker or partially overlapped with the diffraction ring of the WN phase.

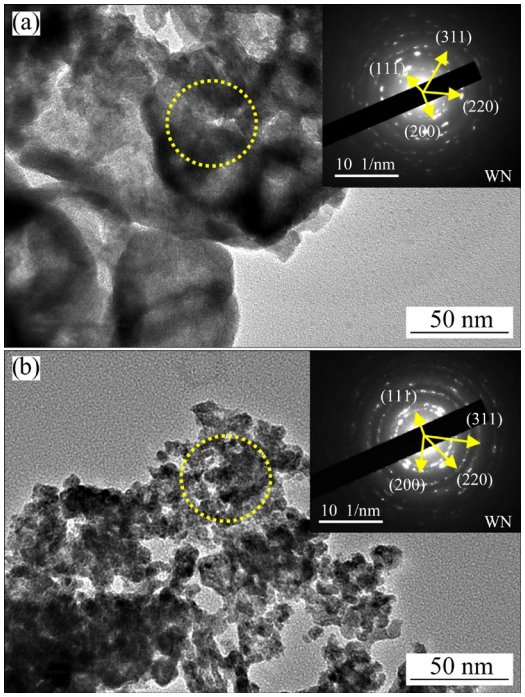

Fig. 8 TEM images and polycrystalline diffraction patterns of $(NH_4)_{0.42}WO_3$/WN (a) and $(NH_4)_{0.42}WO_3$/WN−As (b)

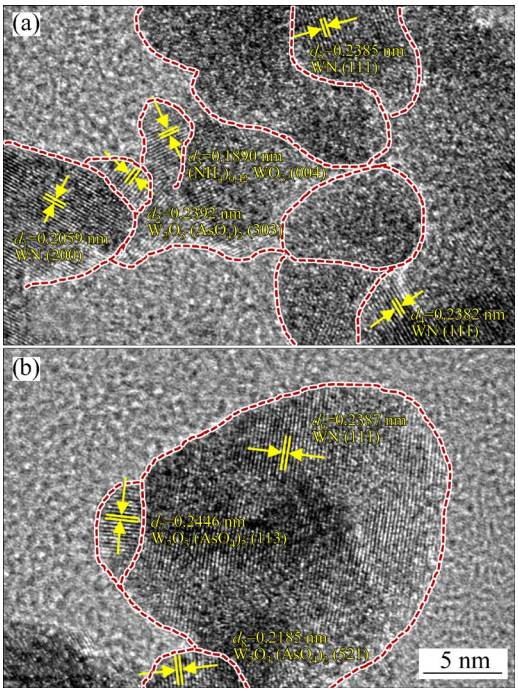

Fig. 9 HRTEM images of $(NH_4)_{0.42}WO_3$/WN−As

To reveal the distribution of $(NH_4)_{0.42}WO_3$/WN and As-containing phases, the $(NH_4)_{0.42}WO_3$/WN−As composite powder was analyzed by high resolution transmission electron microscopy (HRTEM). In Fig. 9, the crystal plane d_1=0.2059 nm, which belongs to the (200) crystal plane of WN. The crystal planes d_4=0.2382 nm, d_5=0.2385 nm and d_6=0.2387 nm are close to the standard crystal plane spacing d=0.2384 nm corresponding to the (111) crystal plane of WN, so d_4, d_5 and d_6 are judged to be the (111) crystal plane of WN. Similarly, d_3=0.1890 nm, corresponding to the (004) crystal plane of $(NH_4)_{0.42}WO_3$. The three crystal planes d_2=0.2392 nm, d_7=0.2446 nm and d_8=0.2185 nm correspond to the (303), (113) and (521) crystal planes of $W_2O_3(AsO_4)_2$, respectively. $W_2O_3(AsO_4)_2$ is distributed between WN and $(NH_4)_{0.42}WO_3$ particles, which can effectively hinder the growth of WC particles during carbonization. In addition, $(NH_4)_{0.42}WO_3$ is distributed between WN particles, which separates WN particles well. Similarly, WN also has an isolation effect on $(NH_4)_{0.42}WO_3$. This phase distribution of WN and $(NH_4)_{0.42}WO_3$ will form a good barrier effect in the subsequent direct carbonization of WC.

Figure 10 shows the process of preparing WC powder by direct carbonization of different nitrided products based on the above experimental results. Figure 10(a) describes the direct carbonization process of the product $(NH_4)_{0.25}WO_3$ obtained by nitrided APT at 500 °C. After ball milling, the surface of $(NH_4)_{0.25}WO_3$ is wrapped by carbon black. Carbon atoms diffuse from the surface to the interior of $(NH_4)_{0.25}WO_3$ particles, NH_4^+ is gradually decomposed, and oxygen atoms gradually combine with C to form CO or CO_2 with the increase of temperature. After the phase transition process of W→W_2C→WC, all $(NH_4)_{0.25}WO_3$ is transformed into WC. In this process, the adjacent particles in the system are the same phase $(NH_4)_{0.25}WO_3$ with the same structure. As a result, the carbonization process of the same phase is the same under high temperature conditions. Moreover, WC particles are easy to form sintering necks and grain boundaries during and after the carbonization. Migration occurs to merge and grow grains, thus forming coarse secondary particles. Figure 10(b) shows the direct carbonization process diagram of $(NH_4)_{0.42}WO_3$/WN composite powder obtained by nitridation APT at 600 °C. $(NH_4)_{0.42}WO_3$ and WN are evenly distributed. $(NH_4)_{0.42}WO_3$ belongs to the hexagonal structure, while WN belongs to the face-centered cubic structure. Their lattice constants are also

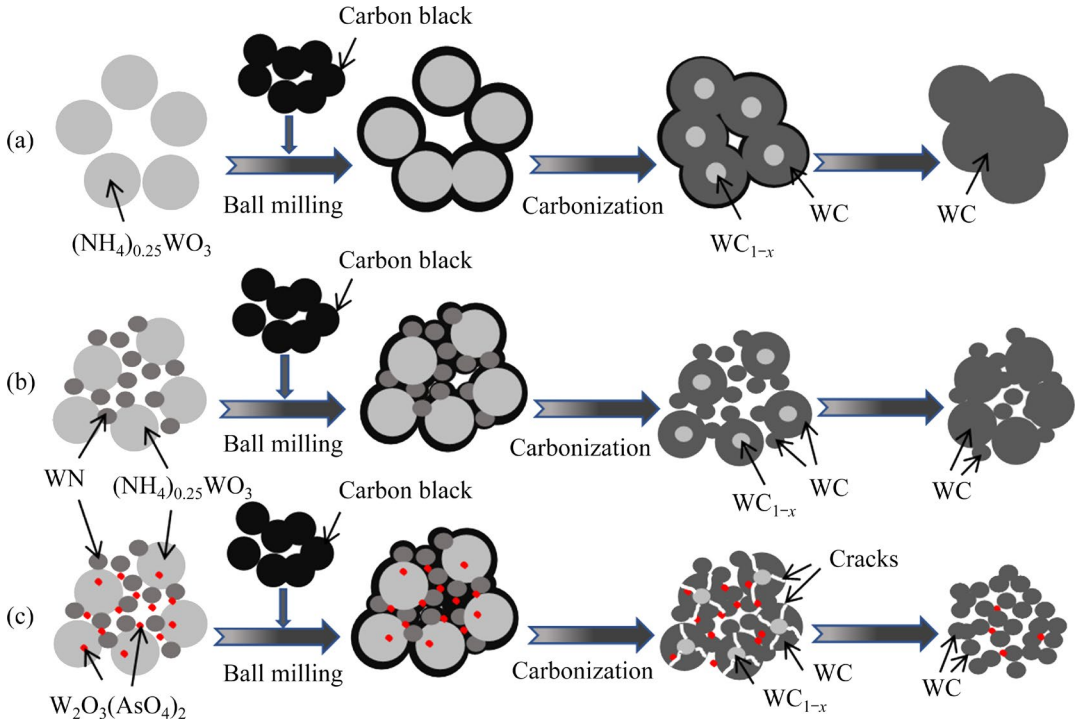

Fig. 10 Schematic diagrams of WC particles growth during direct carbonization of different calcined products: (a) $(NH_4)_{0.25}WO_3$ after calcination of APT at 500 °C; (b) $(NH_4)_{0.42}WO_3$/WN after calcination of APT at 600 °C; (c) $(NH_4)_{0.42}WO_3$/WN−As after calcination of APT−0.3%As at 600 °C

different, which is difficult to form a coherent or semi-coherent interface. The difference between their carbonization processes hinders the migration and growth of WC particles through grain boundary and reduces the growth rate of WC particles, so as to achieve the refinement of WC preparation. Figure 10(c) shows the direct carbonization process diagram of $(NH_4)_{0.42}WO_3$/WN−As composite powder obtained by nitrided APT−As at 600 °C. As element exists in the form of $W_2O_3(AsO_4)_2$ on the surface or inside of $(NH_4)_{0.42}WO_3$ and WN particles. On the one hand, the $W_2O_3(AsO_4)_2$ particles distributed inside the WC particles can form internal stress during the carbonization process, so that the WC particles are broken. On the other hand, the $W_2O_3(AsO_4)_2$ particles distributed on the surface can further inhibit the growth of WC particles by hindering the diffusion of carbon and the growth of adjacent WC particles, and finally the ultrafine WC powders were prepared.

4 Conclusions

(1) The products of precursor APT and APT−0.3%As nitrided at 500 °C in ammonia atmosphere were both $(NH_4)_{0.25}WO_3$, while the products nitrided at 600 °C were $(NH_4)_{0.42}WO_3$ and WN composite powders. At the same nitridation temperature, the particle size of $(NH_4)_{0.25}WO_3$ or $(NH_4)_{0.42}WO_3$/WN containing As was obviously smaller than that without As.

(2) Compared with the direct carbonization of $(NH_4)_{0.25}WO_3$ single phase, the average particle size of tungsten carbide prepared by direct carbonization of $(NH_4)_{0.42}WO_3$/WN composite powder was significantly reduced, and the average particle size of WC was reduced from 2.23 to 0.43 μm. The reason is that the $(NH_4)_{0.42}WO_3$/WN composite powders are evenly distributed and the two phases are separated from each other, which hinders the migration and coalescence of WC grains through grain boundaries during carbonization.

(3) The addition of As element further promotes the refinement of WC powder. As exists in the form of $W_2O_3(AsO_4)_2$ in the $(NH_4)_{0.42}WO_3$/WN composite powders and is easily enriched on the surface of $(NH_4)_{0.42}WO_3$ and WN or distributed between $(NH_4)_{0.42}WO_3$ and WN phases. During the carbonization process, it further hinders the merger and growth of WC grains.

CRediT authorship contribution statement

Zhi-qiang YI: Data curation, Methodology, Software, Writing − Original draft; **Dun-qiang TAN:** Supervision, Project administration, Conceptualization, Writing − Review & editing.

Declaration of competing interest

The authors declare that they have no known competing financial interests or personal relationships that could have appeared to influence the work reported in this paper.

Acknowledgments

This research was supported by the National Natural Science Foundation of China (Nos.52164043, 51564036), and the Special Fund Project for Postgraduate Innovation in Jiangxi Province, China (No. YC2020-B008).

References

[1] LIU Wen-bin, SONG Xiao-yan, ZHANG Jiu-xing, YIN Fu-xing, ZHANG Guo-zhen. A novel route to prepare ultrafine-grained WC−Co cemented carbides [J]. Journal of Alloys and Compounds, 2008, 458(1/2): 366−371.

[2] LIU Kui, WANG Zhen-hua, YIN Zeng-bin, CAO Li-yan, YUAN Jun-tang. Effect of Co content on microstructure and mechanical properties of ultrafine grained WC−Co cemented carbide sintered by spark plasma sintering [J]. Ceramics International, 2018, 44(15): 18711−18718.

[3] KLUNSNER T, WURSTER S, SUPANCIC P, EBNER R, JENKO M, GLAETZLE J, PUESCHEL A, PIPPAN R. Effect of specimen size on the tensile strength of WC−Co hard metal [J]. Acta Materialia, 2011, 59(10): 4244−4252.

[4] XIAO Dai-hong, HE Yue-hui, LUO Wei-hong, SONG Min. Effect of VC and NbC additions on microstructure and properties of ultrafine WC−10Co cemented carbides [J]. Transactions of Nonferrous Metals Society of China, 2009, 19(6): 1520−1525.

[5] HU Miao, TANG Jian-cheng, CHEN Xin-gui, YE Nan, ZHAO Xin-yue, XU Miao-miao. Microstructure and properties of WC−12Co composite coatings prepared by laser cladding [J]. Transactions of Nonferrous Metals Society of China, 2020, 30(4): 1017−1030.

[6] YANG Qiu-min, YANG Jian-gao, YANG Hai-lin, NI Guo-hua, RUAN Jian-ming. Synthesis of ultrafine WC−10Co composite powders with carbon boat added and densification by sinter-HIP [J]. International Journal of Refractory Metals & Hard Materials, 2017, 62: 104−109.

[7] ZHANG Li, CHEN Shu, WANG Yuan-jie, YU Xian-wang, XIONG Xiang-jun. Tungsten carbide platelet-containing cemented carbide with yttrium containing dispersed phase [J]. Transactions of Nonferrous Metals Society of China, 2008, 18(1): 104−108.

[8] JAFARI M, ENAYATI M H, SALEHI M, NAHVI S M, PARK C G. Microstructural evolution of nanosized tungsten carbide during heatup stage of sintering of electroless nickel-coated nanostructured WC−Co powder [J]. Ceramics International, 2014, 40(7): 11031−11039.

[9] WANG Kai-fei, YANG Xiao-hui, DENG Xiao-chun, CHOU Kuo-chi, ZHANG Guo-hua. Enhancement of the mechanical properties of ultrafine-grained WC−Co cemented carbides via the in-situ generation of VC [J]. Journal of Alloys and Compounds, 2022, 903: 163961.

[10] MIN Fan-lu, YU Song-bai, WANG Sheng, YAO Zhan-hu, NOUDEM J G, LIU Si-jin, ZHANG Jian-feng. Preparation and properties of Ni-coated WC powder and highly impact resistant and corrosion resistant WC−Ni cemented carbides [J]. Transactions of Nonferrous Metals Society of China, 2022, 32(6): 1935−1947.

[11] DONOSO A A E, PETERS B. XDEM employed to predict reduction of tungsten oxide in a dry hydrogen atmosphere [J]. International Journal of Refractory Metals and Hard Materials, 2015, 49: 88−94.

[12] KARPOVICH N F, LEBUKHOVA N V, ZAVODINSKY V G, MAKAREVICH, K S. Mechanism of the single-crystal tungsten whiskers growth in the process of the $NiWO_4$ reduction by CO [J]. The Journal of Physical Chemistry C, 2008, 112(47): 18455−18458.

[13] MADARASZ J, SZILAGYI I M, HANGE F, POKOL G. Comparative evolved gas analyses (TG-FTIR, TG/DTA-MS) and solid state (FTIR, XRD) studies on thermal decomposition of ammonium paratungstate tetrahydrate (APT) in air [J]. Journal of Analytical and Applied Pyrolysis, 2004, 72(2): 197−201.

[14] LACKNER A, FILZWIESER A, PASCHEN P, KOCK W. On the reduction of tungsten blue oxide in a stream of hydrogen [J]. International Journal of Refractory Metals & Hard Materials, 1996, 14(5/6): 383−391.

[15] YE Nan, TANG Jian-cheng, ZHUO Hai-ou, WU Tong, XUE Ying-yu. Effect of carbon addition on tungsten nanopowders prepared by hydrogen reduction of tungsten oxide [J]. Rare Metal Materials and Engineering, 2016, 45(9): 2403−2408. (in Chinese)

[16] OSTERMANN M, DALBAUER V, SCHUBERT W D, HAUBNER R. Preparation of nano-crystalline tungsten powders from gaseous $WO_2(OH)_2$ [J]. Tungsten, 2022, 4: 60−66.

[17] POLINI R, PALMIERI E, MARCHESELLI G C. Nanostructured tungsten carbide synthesis by carbothermic reduction of scheelite: A comprehensive study [J]. International Journal of Refractory Metals and Hard Materials, 2015, 51: 289−300.

[18] FANG Z Z, WANG X, RYU T, HWANG K S, SOHN, H Y. Synthesis, sintering, and mechanical properties of nanocrystalline cemented tungsten carbide—A review [J]. International Journal of Refractory Metals & Hard Materials, 2009, 27(2): 288−299.

[19] SINGH H, PANDEY O P. Direct synthesis of nanocrystalline tungsten carbide from scheelite ore by solid state reaction method [J]. Ceramics International, 2013, 39(1): 785−790.

[20] WANG Kai-fei, ZHANG Guo-hua. Synthesis of high-purity ultrafine tungsten and tungsten carbide powders [J]. Transactions of Nonferrous Metals Society of China, 2020, 30(6): 1697−1706.

[21] STANCIU V I, VITRY V, DELAUNOIS F. Tungsten carbide

powder obtained by direct carburization of tungsten trioxide using mechanical alloying method [J]. Journal of Alloys and Compounds, 2016, 659: 302−308.
[22] MA J, ZHU S G. Direct solid-state synthesis of tungsten carbide nanoparticles from mechanically activated tungsten oxide and graphite [J]. International Journal of Refractory Metals and Hard Materials, 2010, 28(5): 623−627.
[23] PAN Feng, ZHU Qing-shan, LI Shao-fu, XIANG Mao-qiao, DU Zhan. Decomposition−carbonization of ammonium paratungstate in a fluidized bed [J]. International Journal of Refractory Metals and Hard Materials, 2018, 72: 315−322.
[24] DANG Jie, WU Yi-jie, LV Ze-peng, LV Xue-wei. Preparation of tungsten carbides by reducing and carbonizing WO_2 with CO [J]. Journal of Alloys and Compounds, 2018, 745: 421−429.
[25] WANG Kai-hei, SUN Guo-dong, WU Yue-dong, ZHANG Guo-hua, CHOU Kuo-chi. Size-controlled synthesis of high-purity tungsten carbide powders via a carbothermic reduction–carburization process [J]. International Journal of Refractory Metals and Hard Materials, 2019, 84: 104975.
[26] OSTERMANN M, HAUBNER R. Deposition of nano-crystalline tungsten carbide powders from gaseous $WO_2(OH)_2$ [J]. Tungsten, 2023, 5: 136−144.
[27] ZHANG Tian-rui, CAI Xiao-ping, LIU Lie-wen, ZENG Hai-ping. Research on separation experiment of scheelite, wolframite and cassiterite for a mine [J]. China Mining Magazine, 2014, 23: 242−251. (in Chinese)
[28] LI Yun-jiao, LI Hong-gui, SUN Pei-mei, LIU Mao-sheng, SU Peng-tuan. Effects of calcium on inhibiting impurities leaching during caustic decomposition of tungsten concentrates by mechanical activation method [J]. Chinese Journal of Rare Metals, 2001, 25(2): 103−107. (in Chinese)
[29] LI Hong-gui, YANG Jian-gao, LI Kun. Tungsten metallurgy [M]. Changsha: Central South University Press, 2010: 64−72. (in Chinese)
[30] ZHU Hong-bo, TAN Dun-qiang, LI Ya-lei, YANG Xin, HE Wen. Refining mechanisms of arsenic in the hydrogen reduction process of tungsten oxide [J]. Advanced Powder Technology, 2015, 26(3): 1013−1020.
[31] WANG Xiao-ru, TAN Dun-qiang, ZHU Hong-bo, HE Wen, OUYANG Chun, ZOU Zhi-hang, YI Zhi-qiang, KUANG Hai. Effect mechanism of arsenic on the growth of ultrafine tungsten carbide powder [J]. Advanced Powder Technology, 2018, 29(6): 1348−1356.
[32] ALTAF S, IJAZ H, HAIDER J, NAZ M, AQEEL M, UL-HAMID A, IKRAM M, ZULFIQAR S, DITTA S A, SHAHBAZ A, IKRAM M. Influence of various transition metals incorporated into tellurium used as antimicrobial agent and textile dye degrader [J]. Applied Nanoscience, 2020, 10(11): 4241−4254.

砷在氮化−碳化法制备超细碳化钨粉过程中的细化机理

易志强[1]，谭敦强[1,2]

1. 南昌大学 物理与材料学院，南昌 330031；
2. 南昌大学 国际材料创新研究院，南昌 330031

摘　要：为了简化工艺制备超细 WC 粉末，在伸钨酸铵前驱体中添加一定量的 As 元素，采用氮化−碳化法系统研究 As 在超细 WC 粉制备过程中的作用机理。结果表明，当碳化温度均为 1400 ℃，氮化温度从 500 ℃升高到 600 ℃，As 含量从 0 增加到 0.3% (质量分数) 时，所制备的 WC 粉平均粒径从 2.23 μm 减小到 0.22 μm，颗粒均匀性显著提高。As 元素在氮化产物中以 $W_2O_3(AsO_4)_2$ 的形式存在，且容易在氮化产物 $(NH_4)_{0.42}WO_3$ 和 WN 表面富集或分布于两相之间，阻碍碳化过程中 WC 晶粒的长大，从而制备超细 WC 粉。

关键词：砷；超细 WC 粉；均匀性；细化机理；氮化；碳化

(Edited by Wei-ping CHEN)